ARTICLE

Ionic conduction in ammonia functionalised *closo*-dodecaborates $MB_{12}H_{11}NH_3$ (M = Li and Na)

Received 00th January 20xx,
Accepted 00th January 20xx

DOI: 10.1039/x0xx00000x

Steffen R. H. Jensen[a,b], Mathias Jørgensen[b], Thi Phuong Thao Nguyen[a], Greg Nolan[a], Craig E. Buckley[a], Torben R. Jensen[b]* and Mark Paskevicius[a]*

Metal hydroborates and their derivatives have been receiving attention as potential solid-state ion conductors for battery applications owing to their impressive electrochemical and mechanical characteristics. However, to date only a fraction of these compounds has been investigated as solid-state electrolytes. Here, $MB_{12}H_{11}NH_3$ (M = Li and Na) hydroborates are synthesized and investigated as electrolyte materials for all-solid-state batteries. The room temperature α-$NaB_{12}H_{11}NH_3$ was structurally solved in $P2_12_12_1$ (a = 7.1972(3) Å, b = 9.9225(4) Å, and c = 14.5556(5) Å). It shows a polymorphic structural transition near 140 °C to cubic $Fm\text{-}3m$. $LiB_{12}H_{11}NH_3$ and $NaB_{12}H_{11}NH_3$ exhibit cationic conductivities of $\sigma(Li^+) = 3.0 \times 10^{-4}$ Scm^{-1} and $\sigma(Na^+) = 1.2 \times 10^{-4}$ Scm^{-1} at 200 °C. Hydration is found to improve ionic conductivity of the hydroborates. It is presumed that modest ionic conductivities could be due to a lack of significant re-orientational dynamics in the crystal structure resulting from the presence of the bulky -NH_3 group in the anion.

Introduction

Since their first commercialization in the late 1960s, Li-ion batteries have become an essential part of our daily life, used in a variety of devices from mobile phones to electric vehicles.[1] However, current Li-ion batteries face critical issues in terms of safety due to the use of volatile and flammable liquid organic electrolytes.[2,3] Moreover, it is expensive to scale up Li-ion batteries for applications such as electric vehicles and large-scale stationary energy storage because of high material and manufacturing costs from numerous housing, electrical and thermal components as well as high maintenance and operating costs.[4,5] In recent years, all-solid-state batteries (ASSB) have emerged as promising next generation batteries, which have the potential to provide high energy density while overcoming the problems of traditional Li-ion batteries.[6,7]

ASSBs, similar to conventional batteries, have three main components: a positive electrode (cathode), a negative electrode (anode) and an electrolyte working as a medium providing ionic conductivity between the two electrodes,[8] but the liquid electrolyte is replaced with a solid-state ionic conductor. To date, many materials have been investigated as solid-state electrolytes (SSE) for ASSBs, with some of the popular compounds being metal oxides, sulfide salts, metal borates and polymers.[6,9,10] Among those, metal borates are receiving enormous attention owing to their superionic conductivity, impressive electrochemical and thermal stability, and deformable properties that allow better electrode-electrolyte interfaces in battery fabrication.[6,11,12] Metal borates have long been synthesized and utilized in various scientific fields such as hydrogen storage and manufacture of chemicals and medicinal agents[11,13] but they only started to draw attention as SSEs after 2007, when high Li-ionic conductivity was first reported for $LiBH_4$ by Matsuo *et al*.[14] Since then, many borohydrides and polyhedral borohydrides (hydroborates) have been synthesized and characterized for battery applications. Recent research has focused on metal salts of large cage-like anions such as $B_{12}H_{12}^{2-}$, $B_{10}H_{10}^{2-}$ and $B_{11}H_{14}^{-}$ due to the weakly coordinating nature of large anions.[15–17] $Na_2B_{12}H_{12}$ and $Na_2B_{10}H_{10}$ were shown to exhibit exceptional conductivities on the order of 0.1 Scm^{-1} above their polymorphic phase transition temperatures (255 and 100 °C, respectively).[15,16] Ionic conductivities of 2.4×10^{-4} and 1.2×10^{-3} Scm^{-1} at 25 °C were reported for ball-milled hydrated $LiB_{11}H_{14}$ and $NaB_{11}H_{14}$, which are some of the highest room temperature (RT) conductivities for SSEs.[17] One of the challenges in implementing metal hydroborates in commercial batteries is to widen the effective operating window of the compounds to low temperatures, but maintain the high ionic conductivity. Because the structural dynamics induced by the order-disorder phase transition is the main mechanism behind the superionic conductivity of hydroborates,[6] bringing such transition down to RT has become an interest among researchers, leading to studies of chemically modified hydroborate anions. The phase transition can be brought to lower temperatures by substituting one B atom in the anion cage with a C atom.[18] In contrast, the substitution of H atoms in $Na_2B_{12}H_{12}$ with halogens or OH groups was shown to shift the order-disorder phase transition to higher temperatures and consequently, cause low ionic conductivities at and near RT.[19,20] Beside these chemical modifications, polyhedral borohydride anions can also be functionalized with a variety of functional groups, such as amines, thiols, and oxo groups,[13,21] or by replacing a B-H unit in the cages with a heavy metal atom such as Pb[22] based on the activation

[a] *Department of Physics and Astronomy, Institute for Energy Transitions, Curtin University, GPO Box U1987, Perth, WA 6845, Australia.*
[b] *Department of Chemistry, Interdisciplinary Nanoscience Center (iNANO), Aarhus University, Langelandsgade 140, DK-8000 Aarhus, Denmark.*

† Electronic Supplementary Information (ESI) available: Additional experimental results. Arrhenius and Nyquist impedance plots. See DOI: 10.1039/x0xx00000x

and conversion of the B-H bond.[23] Because of such diversity in possible chemical modifications, to date only a small number of previously synthesised hydroborate-based compounds have been investigated as SSEs.

Here, for the first time, ammonia functionalized *closo*-dodecaborates $MB_{12}H_{11}NH_3$ (M = Li and Na) are investigated as electrolyte materials for ASSBs. The synthesis of the hydroborates is conducted via the amination of $B_{12}H_{12}^{2-}$ with hydroxylamine-O-sulfonic acid. The compounds are characterized with nuclear magnetic resonance (NMR), thermogravimetric analysis and differential scanning calorimetry (TGA-DSC), X-ray diffraction (XRD) and *in-situ* synchrotron X-ray diffraction (SR-XRD). Ionic conductivities of the hydroborates are determined from electrochemical impedance spectroscopy (EIS) measurements. Based on the results, impacts of the NH_3 group on the ionic conductivity behaviour of the cation are discussed. This work is expected to further increase knowledge of metal hydroborate-based SSEs and gain more insight into the influence of functional groups to ionic conductivity of these compounds.

Experimental

Ammonia functionalized *closo*-dodecaborates $MB_{12}H_{11}NH_3$ (M = Li and Na) are synthesized by amination of $B_{12}H_{12}^{-2}$ with hydroxylamine-O-sulfonic acid, based on a method previously reported by Hertler *et al*.[21] with adaptations.

Synthesis of $Na_2B_{12}H_{12}$. $Na_2B_{12}H_{12}$ is synthesized from $NaBH_4$ via $NaB_{11}H_{14}$ in a two-step reaction. Firstly, $NaB_{11}H_{14}{\cdot}(C_6H_{14}O_3)_n$ is synthesized by reacting $NaBH_4$ (Alfa Aesar, 98%) with 1-bromopentane ($C_5H_{11}Br$, Sigma-Aldrich, 98%) at a $NaBH_4$-to-$C_5H_{11}Br$ molar ratio of 11:10 in diglyme ($C_6H_{14}O_3$, Sigma-Aldrich, 99.5%) at ca. 105 °C for 12 h. Details of the synthesis procedure have been described elsewhere.[17,24] Solvated $NaB_{11}H_{14}$ is isolated by filtrating the resulting solution and evaporating the diglyme solvent under vacuum on the Schlenk line. Then, a mixture of the $NaB_{11}H_{14}$ and $NaBH_4$ at a molar ratio of 1:1 is dissolved in diglyme and heated to ca. 160 °C to reflux for 3 h. The resulting suspension is cooled to RT and the precipitate, which contains $Na_2B_{12}H_{12}$,[25] is filtered and washed with diglyme and flushed multiple times with tetrahydrofuran (THF, Sigma-Aldrich, 99%). The portion soluble in THF ($Na_2B_{12}H_{12}$) is collected by evaporating the solvent in a rotary evaporator following by drying at 100 °C under dynamic vacuum on the Schlenk line before being stored under argon.

Synthesis of $MB_{12}H_{11}NH_3$ (M = Li and Na). $Na_2B_{12}H_{12}$ is dissolved in milli-Q water and then the resulting solution is heated to reflux. An aqueous solution of hydroxylamine-O-sulfonic acid (H_3NO_4S, Sigma-Aldrich, 97%) in milli-Q water is added dropwise to the refluxing solution while stirring (H_3NO_4S:$Na_2B_{12}H_{12}$ = 2:1). After the addition is completed, the solution is allowed to reflux for additional 3 h. $B_{12}H_{11}NH_3^-$ is formed from the reaction of $B_{12}H_{12}^{2-}$ with hydroxylamine-O-sulfonic acid in aqueous solution:

$$B_{12}H_{12}^{2-} + H_2NOSO_3^- \rightarrow B_{12}H_{11}NH_3^- + SO_4^{2-} \qquad (1)$$

and three isomers of $B_{12}H_{10}(NH_3)_2$ (1,7-$B_{12}H_{10}(NH_3)_2$, 1,2-$B_{12}H_{10}(NH_3)_2$ and 1,12-$B_{12}H_{10}(NH_3)_2$) can also be formed as by-products.[21] The resulting suspension is cooled to RT and filtered. Solid products remaining on the filter ($NaB_{12}H_{11}NH_3$, Na_2SO_4, $B_{12}H_{10}(NH_3)_2$ and $Na_2B_{12}H_{12}$) are collected and dried at 80 °C under dynamic vacuum. $B_{12}H_{11}NH_3^-$ is extracted as $MB_{12}H_{11}NH_3$ (M = Li and Na) using the following procedures.

To synthesize $LiB_{12}H_{11}NH_3$, firstly $NaB_{12}H_{11}NH_3$ is isolated by precipitation and liquid-liquid extraction.[26] Sulphate, SO_4^{2-} is removed via the precipitation of Na_2SO_4 in a water/ethanol (Labserv, 99.5%) solution. After the remaining solution is dried in a rotary evaporator, the obtained solid is dissolved in milli-Q water and the $B_{12}H_{10}(NH_3)_2$ is removed by washing the solution with ethyl acetate (Sigma-Aldrich, 99.8%). The aqueous layer is dried at 80 °C under dynamic vacuum to remove water and then, acetonitrile (MeCN, Sigma-Aldrich, 99.8%, Me = methyl, $–CH_3$) is added to extract the $NaB_{12}H_{11}NH_3$. After MeCN is removed by applying dynamic vacuum at RT, the resulting $NaB_{12}H_{11}NH_3$ is dissolved in milli-Q water and the solution is passed through an ion exchange resin (amberlite IR120-H, Fluka). An aqueous solution of lithium hydroxide (LiOH, Alfa Aesar, 98%) is added dropwise until neutral pH. Then, water is evaporated using a rotary evaporator and MeCN is added to separate $LiB_{12}H_{11}NH_3$ from any excess LiOH. $LiB_{12}H_{11}NH_3{\cdot}x$MeCN is obtained by drying the $LiB_{12}H_{11}NH_3$/MeCN solution at RT under dynamic vacuum on the Schlenk line (XRD data in Figure S1).

$NaB_{12}H_{11}NH_3$ is obtained using a method reported by Bolli *et al*.[27] The crude product from the reaction of $Na_2B_{12}H_{12}$ with hydroxylamine-O-sulfonic acid is dissolved in an aqueous solution of triethylamine (TEA, Sigma-Aldrich, 99.5%). Sodium sulphate, Na_2SO_4 is filtered out after precipitation. The TEA and water are removed using a rotary evaporator. The solid product (a mixture of $NH(CH_2CH_3)_3B_{12}H_{11}NH_3$, $B_{12}H_{10}(NH_3)_2$, and $(NH(CH_2CH_3)_3)_2B_{12}H_{12}$) is dissolved in MeCN. The portion insoluble in MeCN ($B_{12}H_{10}(NH_3)_2$ and $(NH(CH_2CH_3)_3)_2B_{12}H_{12}$) is filtered out and the filtrate is dried at RT under dynamic vacuum to obtain $NH(CH_2CH_3)_3)B_{12}H_{11}NH_3$. After that, stoichiometric amounts of NaOH (Sigma-Aldrich, 98%) and the $NH(CH_2CH_3)_3)B_{12}H_{11}NH_3$ are dissolved together in milli-Q water. The resulting solution is heated at 90 °C under dynamic vacuum to evaporate TEA and water. The white solid product obtained here is referred to as $NaB_{12}H_{11}NH_3{\cdot}xH_2O$.

Dry and solvent-free $MB_{12}H_{11}NH_3$ (M = Li and Na) samples are obtained by further drying the $LiB_{12}H_{11}NH_3{\cdot}x$MeCN and $NaB_{12}H_{11}NH_3{\cdot}xH_2O$ at 220 °C overnight under dynamic vacuum (XRD data in Figure S2). The final white powders are stored in an argon glovebox (MBraun, $p(H_2O, O_2) < 1$ ppm).

Characterization. NMR spectra of the final $MB_{12}H_{11}NH_3$ hydroborates were collected using a Bruker Avance III 400 MHz spectrometer (^{1}H: acetonitrile-d3 (CD_3CN), 400.1 MHz; ^{11}B: CD_3CN, 128.4 MHz; $^{11}B\{^1H\}$: CD_3CN, 128.4 MHz) with $OEt_2{\cdot}BF_3$ as a reference for the ^{11}B spectra.

A PerkinElmer STA 6000 was employed to perform TGA-DSC analysis on $LiB_{12}H_{11}NH_3{\cdot}x$MeCN and $NaB_{12}H_{11}NH_3{\cdot}xH_2O$. Samples (ca. 15 mg) were packed in alumina (Al_2O_3) crucibles under an Ar atmosphere and measured under flowing argon (40 mL/min), but briefly exposed to air during loading into the instrument. Samples were first heated

to 300 °C (10 °C/min) to observe desolvation, cooled down to 40 °C (10 °C/min) before a second heating step up to 600 °C (10 °C/min).

Temperature programmed desorption (TPD) was undertaken by sealing powder samples (~ 20 mg) in a Swagelok cell and performing a thermal ramp using a tube furnace ($\Delta T/\Delta t$ = 5 °Cmin^{-1}) whilst under high vacuum (< 1 × 10^{-4} mbar). Evolved gases were detected by a quadrupole mass spectrometer (Stanford Research Systems, RGA-300).

XRD measurements were performed on a Rigaku Smart Lab diffractometer with a Cu Kα_1 radiation source (λ = 1.540593 Å) and a convergent beam multilayer mirror. Diffractograms were collected at 2θ = 5 – 50° with a scan rate of 1 – 3 °min^{-1} by a Rigaku D/tex detector. All samples were prepared in a glovebox and mounted in 0.5 mm borosilicate capillaries and sealed with glue to prevent exposure to the atmosphere.

In-situ SR-XRD diffractograms of the solvent-free $LiB_{12}H_{11}NH_3$ and $NaB_{12}H_{11}NH_3$ were obtained at the MS–XO4SA beamline at the Swiss Light Source, Paul Scherrer Institute, Villigen, Switzerland. Data were collected using a Mythen II detector with a wavelength of 0.70848 Å. The $LiB_{12}H_{11}NH_3$ and $NaB_{12}H_{11}NH_3$ samples were packed in 0.5 mm seal borosilicate capillaries and heated to 460 and 510 °C, respectively, at $\Delta T/\Delta t$ = 5 °Cmin^{-1} under an Ar atmosphere. Indexing and structure solution was undertaken using Topas v.5 (Bruker) or Free Objects for Crystallography (FOX).[28] A rigid body was used for the $B_{12}H_{11}NH_3^-$ anion and structural refinement for α-$NaB_{12}H_{11}NH_3$ was undertaken on a single anion and cation in $P2_12_12_1$ by refining only the translational parameters and anion rotational parameters after indexing was complete.

EIS measurements were performed using two potentiostats. A BioLogic MTZ-35 impedance analyser was used with an air-tight HTSH-1100 sample holder. Measurements were conducted on solvated samples with 1 mm-thick, 6.35 mm-diameter pellets sandwiched between 0.1 mm gold foil under an Ar atmosphere. Temperature was controlled by an HTF-1100 furnace and monitored by a K-type thermocouple positioned 5 mm from the sample. EIS was conducted at 50 mV AC and 0.1 – 3.5 × 10^6 Hz. Ion conductivity of the metal borates is derived from the impedance data using the *x*-intercept of the semi-circle on a Nyquist impedance plot (Fig. S3†).[19] EIS spectra of the dry solvent-free samples were recorded at 50 mV AC from 1 – 1 × 10^6 Hz using a ZIVE SP1 electrochemical workstation. These measurements were conducted as above in a tube furnace and a PTFE Swagelok-type cell with stainless steel electrodes.

Results and discussion

Synthesis and thermal characterization. The synthesis of ammonia functionalised *closo*-dodecaborates is accomplished by aminating $B_{12}H_{12}^{2-}$ in a reaction with the electrophilic reagent hydroxylamine-O-sulfonic acid.[21] The $Na_2B_{12}H_{12}$ precursor is first synthesized from $NaBH_4$ via $NaB_{11}H_{14}$ in a simplified two-step route adapted from literature.[17,24,25] Fig. S4† shows the $^{11}B\{^1H\}$ NMR spectrum of the as-synthesized $Na_2B_{12}H_{12}$ in D_2O with a major resonance at -15.5 ppm from $B_{12}H_{12}^{2-}$.[29] $^{11}B\{^1H\}$ NMR spectra of the $MB_{12}H_{11}NH_3$ (M = Li and Na) hydroborates after synthesis and drying at 220 °C are provided in Fig. 1(a) and (b). As-synthesised $LiB_{12}H_{11}NH_3$ displays three main resonances at -7.3, -15.8 and -18.9 ppm and weaker resonances at -15.3 and -16.3 ppm (Fig. 1(a)). The three major resonances are in agreement with $B_{12}H_{11}NH_3^-$ reported in the literature with δ = -7.3 ppm for B^1NH_3, δ = -15.8 ppm for $B^{2-11}H$ and δ = -18.9 for $B^{12}H$.[27] The remaining two weaker resonances are from minor impurities. The twelve equivalent borons in $B_{12}H_{12}^{2-}$ give a resonance at ca. -15.5 ppm.[29] It has also been noted that an NMR-detectable amount of the 1,2-$B_{12}H_{10}(NH_3)_2$ isomer can remain after extraction.[26] Thus, for $LiB_{12}H_{12}NH_3$, the resonances at δ = -15.3 and -16.3 ppm may be related to $Li_2B_{12}H_{12}$ (1 mol.%) and 1,2-$B_{12}H_{10}(NH_3)_2$ (11 mol.%) impurities in the sample, where quantitative analysis is based on peak integration considering only B species. In case of $NaB_{12}H_{11}NH_3$,

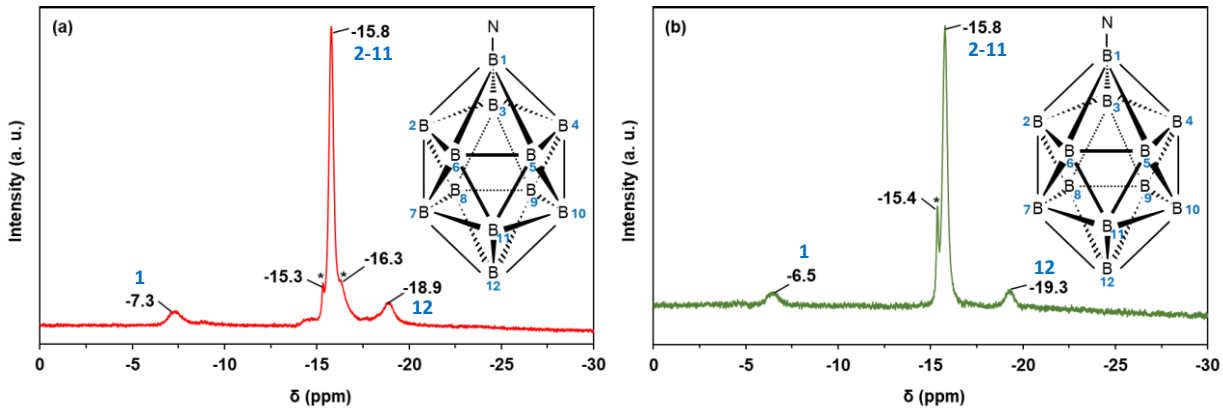

Fig. 1 $^{11}B\{^1H\}$ NMR spectra of (a) $LiB_{12}H_{11}NH_3$ and (b) $NaB_{12}H_{11}NH_3$, acetonitrile-d3 (CD_3CN). *: Impurities. A structure of the $B_{12}H_{11}NH_3^-$ anion is shown with H atoms omitted for clarity.

the presence of $B_{12}H_{11}NH_3^-$ is shown by resonances at chemical shifts of -6.5, -15.8 and -19.3 ppm (Fig. 1(b)). A narrow peak at -15.4 ppm is also observed for this sample and is assigned to $B_{12}H_{12}^{2-}$ impurity (8 mol.%) from the wet synthesis.

Thermogravimetric (TGA) analysis of $LiB_{12}H_{11}NH_3{\cdot}x$MeCN and $NaB_{12}H_{11}NH_3{\cdot}xH_2O$ (Fig. S5†) show mass loss steps at temperatures below 220 °C, assigned to desolvation, when the samples are heated from RT to 300 °C. No further mass loss is detected in the cooling stage. In the second heating step (to 600 °C), mass loss from the $LiB_{12}H_{11}NH_3{\cdot}x$MeCN and $NaB_{12}H_{11}NH_3{\cdot}xH_2O$ is observed from 300 – 400 °C, signifying further desolvation or decomposition of the hydroborates. This analysis is supported by the detection of MeCN and water below 220 °C and traces of hydrogen and ammonia at higher temperatures in mass spectrometry measurements under vacuum using TPD (Fig. S6†). The degree of solvation was measured

from TGA to be $LiB_{12}H_{11}NH_3$·MeCN and $NaB_{12}H_{11}NH_3$·$4H_2O$. Differential scanning calorimetry (DSC) plots (solid lines) for the $LiB_{12}H_{11}NH_3$ and $NaB_{12}H_{11}NH_3$ in the second heating step (after desolvation) are provided in Fig. 2. Both samples show endothermic events above 250 °C, which correspond well with decomposition mass loss steps in their TG curves (dotted lines). Of particular interest are the endothermic events at 150 and 170 °C for $LiB_{12}H_{11}NH_3$ and at 148 °C for $NaB_{12}H_{11}NH_3$ occurring without mass

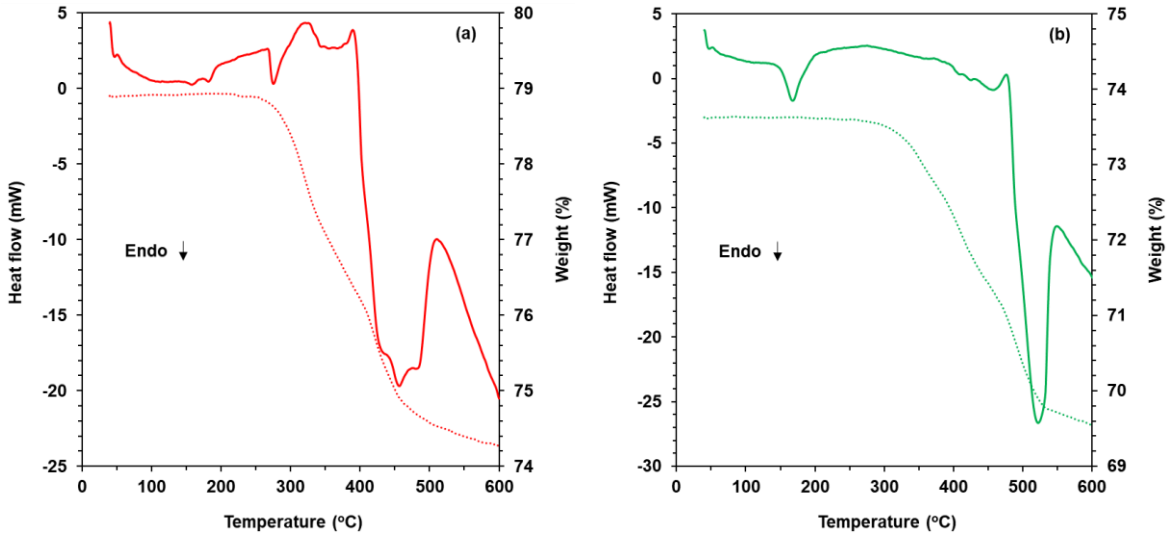

Fig. 2 TGA-DSC plots for (a) $LiB_{12}H_{11}NH_3$ and (b) $NaB_{12}H_{11}NH_3$ in the second heating step (after desolvation). Solid lines: DSC and dotted lines: TGA plots (the starting wt.% relates to the desolvated compounds).

loss. These signals can represent polymorphic phase transitions of the solvent-free $MB_{12}H_{11}NH_3$. The polymorphic transitions are further studied with XRD and SR-XRD and discussed below.

Structural characterization. XRD patterns for the solvent-free $MB_{12}H_{11}NH_3$ collected at RT are provided in Fig. S7.† *In-situ* SR-XRD results for the $LiB_{12}H_{11}NH_3$ during heating are presented in Fig. 3. $LiB_{12}H_{11}NH_3$ experiences polymorphic phase transition (α – β) between 90 and 135 °C, evidenced by the sudden shift of Bragg reflections to lower 2θ, indicative of a substantial volume increase of the unit cell, along with some variation in peak intensities, particularly in regards to the disappearance of minor peaks (Fig. 3). Around 370 °C a noticeable decrease in intensity of the Bragg reflections is observed, indicating thermal decomposition of β-$LiB_{12}H_{11}NH_3$, as corroborated by TGA-DSC and TPD. It is interesting to note that the XRD pattern for α-$LiB_{12}H_{11}NH_3$ is similar to that of α-$Li_2B_{12}H_{12}$, which exists in *Pa*-3 (a = 9.5771 Å) but $Li_2B_{12}H_{12}$ has a polymorphic phase transition at 355 °C.[30,31] The α-$LiB_{12}H_{11}NH_3$ XRD pattern demonstrates peak doubling around the major reflections indicating a loss of symmetry from the cubic α-$Li_2B_{12}H_{12}$ analogue, so a similar crystal structure is expected but could not be solved. It may be easier to solve the structure from single crystal XRD data if a crystal could be grown. The lower temperature of the polymorphic transition in $LiB_{12}H_{11}NH_3$ compared to $Li_2B_{12}H_{12}$ may be related to the anisotropic structure of the anion, due to NH_3 functionalisation, which results in a slightly larger unit cell.

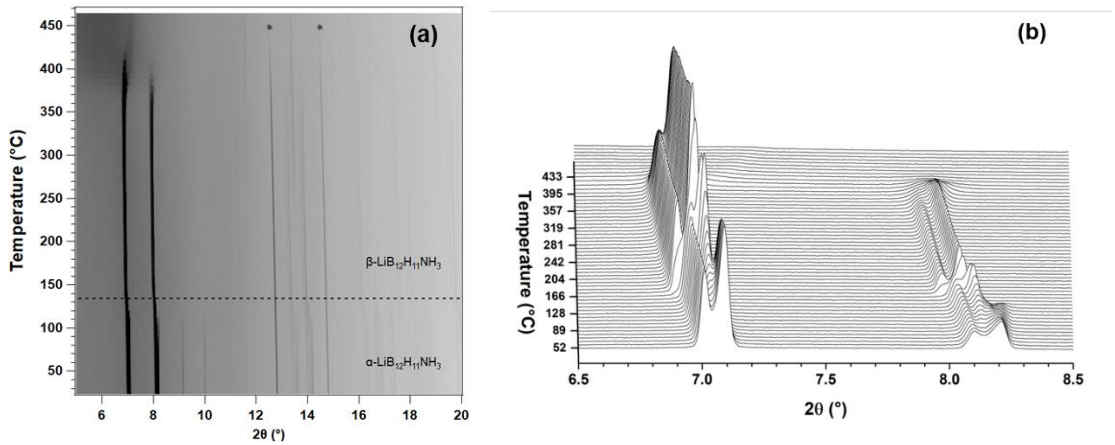

Fig. 3 *In-situ* SR-XRD plots for $LiB_{12}H_{11}NH_3$ upon heating from RT to 460 °C under Ar atmosphere ($\Delta T/\Delta t$ = 5 °Cmin^{-1}, λ = 0.70848 Å). * LiBr impurity.

For $NaB_{12}H_{11}NH_3$, a polymorphic phase transition (α → β) is observed at about 140 °C (Fig. 4) that correlates well with the endothermic event observed from DSC. At room temperature there is a minor quantity of β-$NaB_{12}H_{11}NH_3$ present, which overlaps with some α-

$NaB_{12}H_{11}NH_3$ diffraction peaks. However, α-$NaB_{12}H_{11}NH_3$ was still able to be indexed in $P2_12_12_1$ (a = 7.1972(3) Å, b = 9.9225(4) Å, and c = 14.5556(5) Å) and structurally solved (Fig. 5, Table S1†, COD #3000468). Each Na^+ cation is coordinated to three $B_{12}H_{11}NH_3^-$ anions in a trigonal planar arrangement with bidentate bonding to two hydrogen atoms from each anion. Despite the higher electronegativity of NH_3 group compared to H, Na^+ cations do not coordinate with the NH_3 groups, which form a staggered network through the crystal opposed to the cation positions. Na-H distances are 2.06 – 2.84 Å, which are similar to the Na-H distances reported for $Na_2B_{12}H_{12}$.[32] Due to the chemical similarity, it is interesting to draw comparisons between α-$NaB_{12}H_{11}NH_3$ and $NaB_{12}H_{12}$.[32] The latter is monoclinic in $P2_1/n$ and exhibits Na-Na distances from 4.485 – 5.295 Å, whereas in α-$NaB_{12}H_{11}NH_3$ the Na-Na distances are much larger at 5.601 Å. These differences in cation distance could have implications for the ion conductivity. α-$NaB_{12}H_{11}NH_3$ undergoes a polymorphic phase change to a higher symmetry structure in a similar way to $Na_2B_{12}H_{12}$, which transitions from $P2_1/n$ to Pm-3n at 256 °C, then Im-3m at higher temperatures.[33,34] For α-$NaB_{12}H_{11}NH_3$ the transition occurs at a much lower temperature (140 °C) to β-$NaB_{12}H_{11}NH_3$ that is indexed in Fm-3m (a = 10.3534(7) Å). Interestingly, Verdal *et al.* noted a minor face-centred cubic phase in their structural study of $Na_2B_{12}H_{12}$ polymorphism with a similar lattice parameter (10.41 Å).[34] For β-$NaB_{12}H_{11}NH_3$ this is the only polymorph present. From ~ 425 °C, a large decrease in the unit cell parameters and broadening of the Bragg reflections is observed, suggesting the decomposition of the sample, which is in a good agreement with the TGA-DSC results.

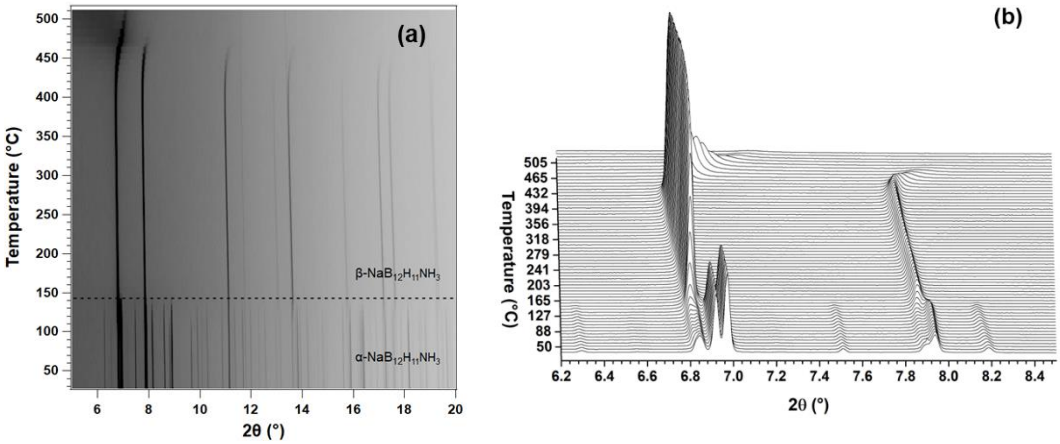

Fig. 4 *In-situ* SR-XRD plots for $NaB_{12}H_{11}NH_3$ upon heating from RT to 510 °C under Ar atmosphere ($\Delta T/\Delta t$ = 5 °Cmin^{-1}, λ = 0.70848 Å).

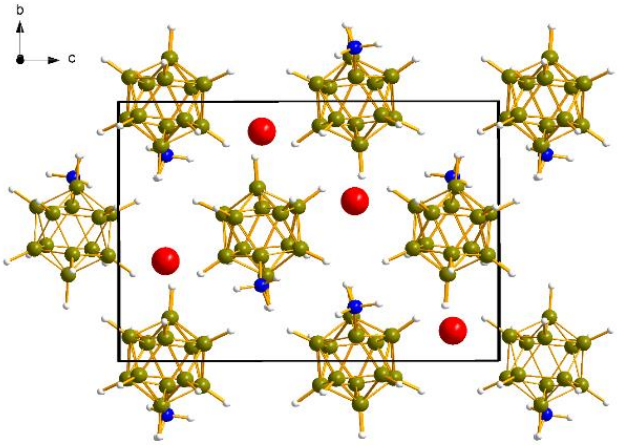

Fig. 5 Crystal structure of α-$NaB_{12}H_{11}NH_3$ in $P2_12_12_1$ (a = 7.1972(3) Å, b = 9.9225(4) Å, and c = 14.5556(5) Å) down the a-axis with red: sodium (Na), blue: nitrogen (N), yellow: boron (B), and white: hydrogen (H).

Ionic conductivity. Ionic conductivity of the $MB_{12}H_{11}NH_3$ (M = Li and Na) hydroborates collected as a function of temperature is provided in Fig. 6. Data were collected for the desolvated $MB_{12}H_{11}NH_3$ along with the hydrated $MB_{12}H_{11}NH_3$ prior to drying at 220 °C under vacuum. The superionic conductivity of hydroborates is widely accepted to strongly correlate with the polymorphic transition to a crystal structure showing dynamics, especially in reorientation of the large weakly coordinating anion.[15,31,35] Experimental and theoretical studies have shown that the transition from low temperature ordered to high temperature disordered polymorph enhances cation diffusion within the materials and thus, leads to a jump in ionic conductivity.[15,31,35] It is surprising to us that such a sharp change in conductivity is not observed for both $LiB_{12}H_{11}NH_3$ and $NaB_{12}H_{11}NH_3$ at temperatures of phase transitions indicated by TGA-DSC and *in-situ* SR-XRD measurements (~ 140 °C). When dried of solvent, $LiB_{12}H_{11}NH_3$ and $NaB_{12}H_{11}NH_3$ show cationic conductivities of $\sigma(Li^+)$ = 8.2 × 10^{-8} Scm^{-1} and $\sigma(Na^+)$ = 4.2 × 10^{-8} Scm^{-1} at 75 °C, respectively. The ionic conductivity of both samples is observed to increase almost linearly with the temperature and reaches $\sigma(Li^+)$ = 3.0 × 10^{-4} Scm^{-1} for $LiB_{12}H_{11}NH_3$ and $\sigma(Na^+)$ = 1.2 × 10^{-4} Scm^{-1} for $NaB_{12}H_{11}NH_3$ at 200 °C. The key to understanding the linear temperature dependency of the ionic conductivity may be in the anion dynamics in the high temperature polymorphs, which may not be present for these functionalised anions, or may not be sufficiently dynamic to provide a step-function change in activation energy for cation migration through the structure. It should be noted that the $B_{12}H_{11}NH_3^-$ anion is monovalent unlike the $B_{12}H_{12}^{2-}$ anion. Although, this means the anion is less negatively charged, and more weakly coordinating like $CB_{11}H_{12}^-$, it also means that the ammoniated salt has a lower cation

concentration. As mentioned previously, monovalent α-$NaB_{12}H_{11}NH_3$ does show much larger Na-Na jump distances than divalent $Na_2B_{12}H_{12}$, in part due to the lower Na concentration in the crystal structure. The linear trend in ionic conductivity may have to be investigated further by direct anion dynamic studies using either nuclear magnetic resonance (NMR) or inelastic neutron scattering (INS).

Interestingly, the hydrated $LiB_{12}H_{11}NH_3$ and $NaB_{12}H_{11}NH_3$ samples show higher ionic conductivity compared with their dehydrated analogues, especially in the case of $LiB_{12}H_{11}NH_3$. The hydrated $LiB_{12}H_{11}NH_3$ sample shows a conductivity of 1.6×10^{-6} Scm^{-1} at 75 °C, which is more than 10 times that shown by its desolvated analogue at the same temperature. At 100 °C, the conductivity measured for this sample is 2.8×10^{-5} Scm^{-1}, which is higher than that reported for $LiBH_4$.[14] For hydrated $NaB_{12}H_{11}NH_3$, a conductivity of 2.5×10^{-4} Scm^{-1} is obtained at 150 °C. The positive impact of coordinated neutral molecules, such as H_2O and NH_3, on ionic conductivity has been previously reported for metal borohydrides and hydroborates.[17,38–40] Hydrated $LiBH_4$ has been shown to exhibit Li^+ conductivity of 4.89×10^{-4} Scm^{-1} at 45 °C, which is comparable to that of anhydrous $LiBH_4$ at high temperature.[38] $LiB_{11}H_{14}{\cdot}nH_2O$ and $NaB_{11}H_{14}{\cdot}nH_2O$ have been shown to exhibit conductivities of 1.8×10^{-4} and 1.1×10^{-3} Scm^{-1} at 25 °C, which are some of the highest Li^+ and Na^+ conductivities at room temperatures reported for SSEs.[17] Kisu *et al.*[39] investigated divalent conduction in hydrated *closo*-dodecaborate salts of Zn and Mg with water coordination of 0 to 12 and reported exceptional conductivities for $ZnB_{12}H_{12}{\cdot}12H_2O$ and $MgB_{12}H_{12}{\cdot}12H_2O$. Based on structural characterization and NMR measurements, the authors proposed that water molecules coordinate with Zn^{2+} and $B_{12}H_{12}^{2-}$ in

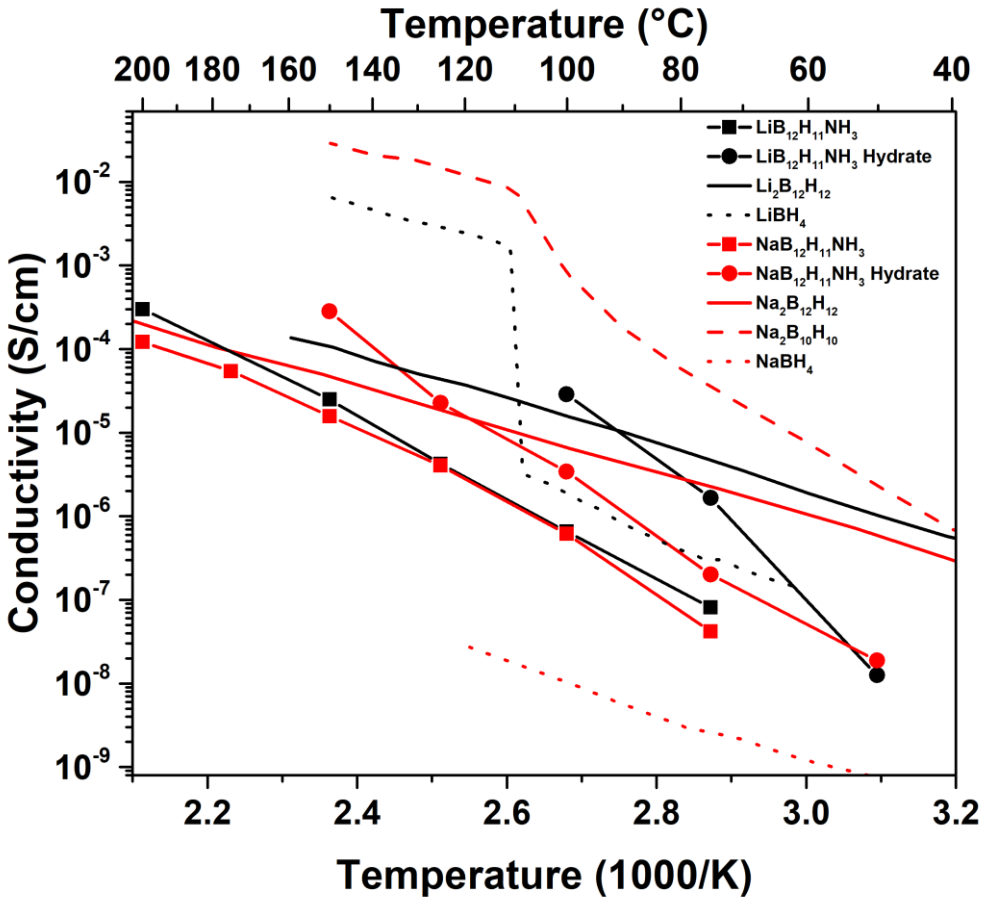

Fig. 6 Ionic conductivity of dry and solvated $LiB_{12}H_{11}NH_3$ and $NaB_{12}H_{11}NH_3$ in comparison to similar compounds: $Li_2B_{12}H_{12}$[36], $LiBH_4$[14], $Na_2B_{12}H_{12}$[15], $Na_2B_{10}H_{10}$[16] and $NaBH_4$.[37] Sodium compounds are in red and lithium compounds in black.

an octahedral coordination that provides large space between the cation and anion easing the rotation of $B_{12}H_{12}^{2-}$ cage and thus leading to Zn^{2+} conduction.[39] They also proposed a rapid exchange of non-coordinated and coordinated H_2O as a mechanism enhancing Zn^{2+} migration.[39] Yan *et al.*[40] studied the mechanism of Mg^{2+} conduction in $Mg(BH_4)_2{\cdot}xNH_3$ with density functional theory calculations and proposed the di-hydrogen bonds between H atoms in BH_4^- anions and the NH_3 molecules as the key to high Mg^{2+} ion mobility in the ammine promoted samples. In similar ways, the coordination with H_2O molecules may facilitate the diffusion of Li^+/Na^+ cations within the crystal structures of the $MB_{12}H_{11}NH_3$ samples leading to the higher conductivities. The ionic conductivity of the solvated $MB_{12}H_{11}NH_3$ analogues above 150 °C could not be measured because of desolvation, as shown in TGA-DSC and TPD results, causing changes in morphology of the electrolyte pellets.

Although the $LiB_{12}H_{11}NH_3$ and $NaB_{12}H_{11}NH_3$ samples have significantly lower polymorphic transition temperatures compared with their respective *closo*-dodecaborates (355 °C[31] and 256 °C[15] for $Li_2B_{12}H_{12}$ and $Na_2B_{12}H_{12}$, respectively), they show no great improvement in ionic conduction compared with the non-modified

compounds. Conductivities comparable to that of $Li_2B_{12}H_{12}$ and $Na_2B_{12}H_{12}$ can only be observed at temperatures above 100 °C. To understand this, we calculate and compare the activation energy of cationic diffusion for the functionalized samples and the un-modified *closo*-dodecaborates from an Arrhenius plot of their ionic conductivity data (Fig. S8†). The activation energies for ionic conduction are 90.7 and 86.8 kJ/mol for the desolvated $LiB_{12}H_{11}NH_3$ and $NaB_{12}H_{11}NH_3$ analogues, and 155.8 and 108.7 kJ/mol for the hydrated $LiB_{12}H_{11}NH_3$ and $NaB_{12}H_{11}NH_3$ analogues, respectively. Meanwhile, the activation energies for $Li_2B_{12}H_{12}$ and $Na_2B_{12}H_{12}$ are 52.2 and 51.6 kJ/mol, which are 1.6 – 3 times lower. These results suggest that it is more difficult for the cations to migrate within the crystal structures containing the ammonia functionalized cage. From geometrical considerations, the ammonia functionalized *closo*-dodecaborates appear to have *fcc* anion packing in their high temperature polymorph, which is structurally similar to $Li_2B_{12}H_{12}$.[31,34] Thus, other factors influence the ionic conductivity of the $MB_{12}H_{11}NH_3$ hydroborates. A clear difference between the ammonia functionalized hydroborates and the un-modified ones is the substitution of one hydrogen atom in the cage with NH_3 group, causing monovalency. As discussed above, the Na-Na distances in α-$NaB_{12}H_{11}NH_3$ are much larger compared with $Na_2B_{12}H_{12}$, in part of lower cation concentration and larger unit cells. This implies that it may be harder for cation jump within the crystal structures of the modified hydroborates, limiting cation diffusion in these compounds. Also, because of the fact that NH_3 is much bulkier than H, there may be restriction of rotation for the $B_{12}H_{11}NH_3^-$ cages, resulting in low rate of anionic rotation after polymorphic transition temperature and thus, hindering the ionic conductivity. However, further experimental and theoretical studies are required to understand the dynamics and ionic conduction characteristics of the ammoniated hydroborate compounds.

Conclusions

Ammonia functionalized *closo*-dodecaborates $MB_{12}H_{11}NH_3$ (M = Li and Na) are investigated as solid-state electrolytes for battery applications. The hydroborate compounds are synthesized via the ammoniation of $B_{12}H_{12}^{2-}$ with hydroxylamine-O-sulfonic acid. Thermal characterization and *in-situ* SR-XRD results show that polymorphic transitions occur at 90 – 135 °C for the functionalized cage, which is significantly lower compared with the respective salts of $B_{12}H_{12}^{2-}$ anion. The $MB_{12}H_{11}NH_3$ hydroborates show an increase in ionic conductivity with increasing temperature without a step-change associated with their polymorphic phase transition. Conductivities of 3.0×10^{-4} and 1.2×10^{-4} Scm^{-1} are obtained for $LiB_{12}H_{11}NH_3$ and $NaB_{12}H_{11}NH_3$ at 200 °C, respectively. Hydration is found to enhance the ionic conductivity of the hydroborates, especially in case of $LiB_{12}H_{11}NH_3$, where the conductivity is observed to increase by more than one order of magnitude. Although the $MB_{12}H_{11}NH_3$ hydroborates have much lower polymorphic transition temperatures they exhibit lower ionic conductivities compared with $Li_2B_{12}H_{12}$ and $Na_2B_{12}H_{12}$. Understanding the dynamic behaviour of the high temperature polymorphs may be key to understand why the ionic conductivity is not as high as expected.

Conflicts of interest

There are no conflicts to declare.

Acknowledgements

The Independent research fund Denmark for technology and production is thanked for funding via the research projects HyNanoBorN (DFF – 4181-00462) and Solid-State Magnesium Batteries – SOS-MagBat (9041-00226B). MP and CEB thanks the Australian Research Council for Discovery Project (DP230100429). MS-XO4SA, Swiss Light Source, Paul Scherrer Institute, Villigen, Switzerland is acknowledged for providing beam time for the *in-situ* experiments.

Notes and references

1 M. V. Reddy, A. Mauger, C. M. Julien, A. Paolella and K. Zaghib, *Materials,* 2020, **13**, 1884–1892.
2 M. R. Malacin and A. de Guibert, *Science*, 2016, **351**, 1253292–1253300.
3 X. Feng, M. Ouyang, X. Liu, L. Lu, Y. Xia and X. He, *Energy Storage Mater*., 2018, **10**, 246–267.
4 A. Kwade, W. Haselrieder, R. Leihoff, A. Modlinger, F. Dietrich and K. Droeder, *Nat. Energy,* 2008, **3**, 290–300.
5 D. H. Doughty, P. C. Butler, A. A. Akhil, N. H. Clark and J. D. Boyes, *Electrochem. Soc. Interface*., 2010, **19**, 49–54.
6 Y. Pang, Y. Liu, J. Yang, S. Zheng and C. Wang, *Mater. Today Nano,* 2022, **18**, 100194–100216.
7 J. Janek and W. G. Zeier, *Nat. Energy,* 2023, **8**, 230–240.
8 M. Winter and R. J. Brodd, *Chem. Rev*. 2004, **104**, 4245–4269.
9 R. Chen, Q. Li, X. Yu, L. Chen and H. Li, *Chem. Rev*., 2020, **120**, 6820–6877.
10 J. Lau, R. H. DeBlock, D. M. Butts, D. S. Ashby, C. S. Choi and B. S. Dunn, *Adv. Energy Mater*., 2018, **8**, 1800933–1800956.
11 R. Cerny, F. Murgia and M. Brighi, *J. Alloys. Compd*., 2002, **895**, 162659–162667.
12 A. Unemoto, M. Matsuo and S. Orimo, *Adv. Funct. Mater*., 2014, **24**, 2267–2279.
13 N. Mahfouz, F. A. Ghaida, Z. E. Hajj, M. Diab, S. Loquet, A. Mehdi and D. Naoufal, *ChemistrySelect,* 2022, **7**, e202200770–e202200785.
14 M. Matsuo, Y. Nakamori, S. Orimo, H. Maekawa and H. Takamura, *Appl. Phys. Lett.,* 2007, **91**, 224103-1–224103-3.
15 T. J. Udovic, M. Matsuo, A. Unemoto, N. Verdal, V. Stavila, A. V. Skripov, J. J. Rush, H. Takamura and S. Orimo, *Chem. Commun.,* 2014, **50**, 3750–3752.
16 T. J. Udovic, M. Matsuo, W. S. Tang, H. Wu, V. Stavila, A. V. Soloninin, R. V. Skoryunov, O. A. Babanova, A. V. Skripov, J. J. Rush, A. Unemoto, H. Takamura and S. Orimo, *Adv. Mater*., 2014, **26**, 7622–7626.
17 D. H. P. Souza, K. T. Moller, S. A. Moggach, T. D. Humphries, A. M. D'Angelo, C. E. Buckley and M. Paskevicius, *J. Mater. Chem. A,* 2021, **9**, 15027–15037.
18 W. S. Tang, A. Unemoto, W. Zhou, V. Stavila, M. Matsuo, H. Wu, S. Orimo and T. J. Udovic, *Energy Environ. Sci.,* 2015, **8**, 3637 – 3645.
19 B. R. S. Hansen, M. Pakevicius, M. Jorgensen and T. R. Jensen, *Chem. Mater*., 2017, **29**, 3423–3430.
20 M. Jorgensen, S. R. H. Jensen, T. D. Humphries, M. R. Rowles, M. V. Sofianos, C. E. Buckley, T. R. Jensen and M. Paskevicius, *J. Phys. Chem. C,* 2020, **124**, 11340–11349.
21 W. R. Hertler and M. S. Raasch, *J. Am. Chem. Soc.,* 1964, **86** (18), 3661–3668.

22 T. A. Hales, K. T. Moller, T. D. Humphries, A. M. D'Angelo, C. E. Buckley and M. Paskevicius, *J. Phys. Chem. C,* 2023, **127**, 949–957.
23 I. B. Sivaev, *Russ. J. Inorg. Chem*. 2021, **66**, 1192–1246.
24 G. B. Dunks, K. Barker, E. Hedaya, C. Hefner, K. Palmer-Ordonez and P. Remec, *Inorg. Chem.,* 1981, **20** (6), 1692–1697.
25 H. C. Miller, N. E. Miller and E. L. Muetterties, *Inorg. Chem.,* 1964, **3** (10), 1456–1463.
26 E. V. Bulovsky, Flourinated Materials Syntheses and Characterization for Energy Storage and Energy Conversion Applications, Colorado State University, 2015.
27 C. Bolli, J. Derendorf, C. Jenne, H. Scherer, C. P. Sindlinger and B. Wegener, *Chem. Eur. J.,* 2014, **20** (42), 13783–13792.
28 V. Favre-Nicolin and R. Cerny, *J. Appl. Cryst*., 2002, **35**, 734–743.
29 K. T. Moller, M. Paskevicius, J. G. Andreason, J. Lee, N. Chen-Tan, J. Overgaard, S. Payande, D. S. Silvester, C. E. Buckley and T. R. Jensen, *Chem. Commun.,* 2019, **55**, 3410–3413.
30 J-H. Her, M. Yousufuddin, W. Zhou, S. S. Jalisatgi, J. G. Kulleck, J. A. Zan, S-J. Hwang, R. C., Jr.[II] Bowman and T. J. Udovic, *Inorg. Chem*., 2008, **47** (21), 9757–9759.
31 M. Paskevicius, M. P. Pitt, D. H. Brown, D. A. Sheppard, S. Chumphongphan and C. E. Buckley, *Phys. Chem. Chem. Phys*., 2013, **15**, 15825–15828.
32 J-H. Her, W. Zhou, V. Stavila, C. M. Brown and T. J. Udovic, *J. Phys. Chem*. C, 2009, **113** (26), 11187–11189.
33 N. Verdal, T. J. Udovic, V. Stavila, W. S. Tang, J. J. Rush and A. V. Skripov, *J. Phys. Chem. C,* 2014, **118** (31) 17483–17489.
34 N. Verdal, J-H. Her, V. Stavila, A. V. Soloninin, O. A. Babanova, A. V. Skripov, T. J. Udovic and J. J. Rush, *J. Solid State Chem*., 2014, **212**, 81–91.
35 K. Sau, T. Ikeshoji, S. Kim, S. Takagi and S. Orimo, *Chem. Mater*., 2021, **33**, 2357−2369.
36 L. He, H-W. Li, H. Nakajima, N. Tumanov, Y. Filinchuk, S-J. Hwang, M. Sharma, H. Hagemann and E. Akiba, *Chem. Mater*., 2015, **27** (16), 5483–5486.
37 M. Matsuo, S. Kuromoto, T. Sato, H. Oguchi, H. Takamura and S. Orimo, *Appl. Phys. Lett*., 2012, **100**, 203904-1–203904-4.
38 A. Takano, I. Oikawa, A. Kamagewa and H. Takamura, *Solid State Ions*., 2016, **285**, 47–50.
39 K. Kisu, A. Dorai, S. Kim, R. Hamada, A. Kumatani, Y. Horiguchi, R. Sato, K. Sau, S. Takagi and S. Orimo, *J. Mater. Chem. A,* 2022, **10**, 24877–24887.
40 Y. Yan, W. Dononelli, M. Jogensen, J. B. Grinderslev, Y-S. Lee, Y. W. Cho, R. Cerny, B. Hammer and T. R. Jensen, *Phys. Chem. Chem. Phys.,* 2020, **22**, 9204–9209.

